Recent Research Developments in Physics

Possible application of the SGMR interferometry to look upon microscopic mechanisms of diffusion in single crystals of partly disordered alloys

Artur Błachowski and Krzysztof Ruebenbauer

Mössbauer Spectroscopy Division, Institute of Physics, Department of Mathematics, Physics and Technology, Pedagogical University
PL-30-084 Kraków, ul. Podchorążych 2, Poland
Electronic address: sfrueben@cyf-kr.edu.pl
WWW: www.cyf-kr.edu.pl/~sfrueben/
Tel.: +(48-12) 662-6317, +(48-12) 662-6319
Fax: +(48-12) 637-2243

Running title: SGMR interferometry

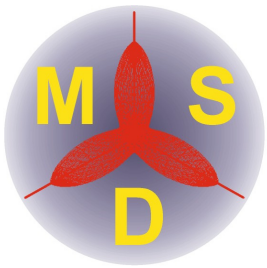

*Contribution to the series **Recent Research Developments in Physics** published by **Transworld Research Network**, Volume 4, Part I, Paper 16, 37/661(2)-16, pp. 333-359 (2003): Fort P.O., Trivandrum-695 023, Kerala, India, http://www.trnres.com , admin@rsflash.com, Tel.: +(91-471) 245-2918, +(91-471) 246-0384, Fax: +(91-471) 257-3051; Managing Editor: S.G. Pandalai; ISBN: 81-7895-078-2. Kraków, February 11th, 2004.*

Kraków

July 10th, 2003

ABSTRACT

The paper is aimed at the review of the present status of the research being done with the help of the synchrotron generated Mössbauer radiation (SGMR). A review is focused on the interferometry performed with the help of the above radiation. Possible applications to the studies of the microscopic mechanisms of diffusion in partly disordered single crystals of alloys are discussed in some detail. A theory of the quasi-elastic Rayleigh scattering by atoms diffusing in the Bravais sub-lattices is outlined followed by the detailed theory of the resonant X-ray interferometer itself. A detailed microscopic model of diffusion in the B2 structure alloys is discussed. Simulated correlation functions and data patterns are shown as well. It is concluded that with the advent of the free electron lasers producing photons of the about 15 keV energy resonant X-ray interferometry is likely to become a powerful tool to look upon rather slow diffusion with a very good spatial resolution enabling to decide between various microscopic models. This method is likely to be applied to materials containing heavy atoms and being able to produce sufficient contrast during scattering at the atomic level. Hence some disorder at the atomic scale must exist in the sample.

INTRODUCTION

Synchrotron radiation generated by the undulators mounted on the high-energy electron or positron storage rings has sufficient luminosity to excite efficiently many Mössbauer levels [1-7]. Hence one can envisage construction of the X-ray interferometers using the above resonant radiation having very narrow energy bandwidth. Such devices have been indeed designed and put into operation [8,9]. Due to the fact that these interferometers rely upon delayed radiation from two resonant targets one has to place the sample investigated between those targets and to use it as a non-resonant scatterer. In order to maintain coherence with the time passing since the prompt pulse exciting resonant targets one has to rely upon elastic or quasi-elastic scattering by the sample. On the other hand, perfectly spatially ordered systems do not scatter elastically beyond the Bragg reflections, as there is no spin and isotopic incoherence in the Rayleigh scattering in contrast to the possible spin and isotopic incoherence in the neutron scattering. This is some drawback as the possible quasi-elastic scattering is due to the diffusion of atoms, and atomic motions of this character are unseen under Bragg conditions, i.e., there is no quasi-elasticity in the radiation scattered into Bragg reflections [10,11]. However disordered samples containing vastly different elements have the ability to scatter incoherently and the latter radiation contains quasi-elastic component. Hence the first applications were concentrated on glasses exhibiting very strong disorder [8]. A natural extension to the crystals (particularly single crystals) is possible with the increasing intensity of the radiation sources. Particularly strong sources are required for small acceptance solid angles required to exploit fully single crystalline properties of the sample and in the limit of the slow diffusion, where resonant targets are to be relatively thin and the separation between subsequent prompt pulses necessarily longer [9]. It seems that the advent of the free electron lasers being capable to excite nuclear resonant levels is going to be a real breakthrough in the application of this method to crystalline matter. This method is characterised by a very good spatial resolution and it is capable to look upon relatively slow diffusion.

The paper is organised as follows: section 1 is devoted to the basic theory of the quasi-elastic scattering of the X-rays by the single crystals exhibiting diffusion of atoms, section 2 deals with the principles of the resonant X-ray interferometry based on the pulsed sources of the

synchrotron radiation. A detailed diffusion model at the atomic level is discussed in the section 3 for partly disordered alloys of the B2 structure. Results of some numerical simulations based on this model are shown in the section 4, while the last section is concerned with the discussion and conclusions.

1. QUASI-ELASTIC DIFFUSIVE SCATTERING OF X-RAYS BY SINGLE CRYSTALS

X-rays are scattered mainly by the electronic shells of atoms constituting scattering material. Other types of scattering could be neglected except the resonant nuclear scattering. It is assumed here that the material investigated is free of the nuclei being able to scatter resonantly within the energy bandwidth of the incoming and outgoing radiation. One can neglect multiple photon processes as well. Hence one has to consider the following processes for typical energies of the incoming X-ray photons provided one is seeking for a photon in the outgoing channel: 1) X-ray fluorescence, 2) Compton scattering and 3) Rayleigh scattering. The X-ray fluorescence and Compton scattering are both inelastic and incoherent processes leading to the outgoing photon having lower energy than the incoming one. Some exception is the Compton scattering at very low scattering angles, where the energy of the outgoing photon approaches energy of the incoming photon in the limit of the forward scattering. On the other hand, the Rayleigh scattering is coherent within the atomic electron shell and elastic within the mass centre co-ordinates defined by the incoming photon and the scattering atom – upon having included recoil energy acquired by the atom. This type of scattering is rather weak and one can neglect multiple scattering as the beam is strongly attenuated by the photo-effect while penetrating into the sample and emerging out of it upon being scattered. The last statement applies to typical X-ray energies. The energy of recoil depends upon the energy of the incoming photon, scattering angle and mass of the scattering atom. It is comparable to the typical phonon energies in the condensed matter. Hence atoms embedded either in the crystalline or amorphous material, the latter having very high viscosity are able to scatter elastically some fraction of the photons. The inelastic component is partly coherent and partly incoherent for crystalline targets, as phonons are not well localised. A coherent part of this component is concentrated in the Bragg reflections. On the other hand, the elastic component is entirely concentrated in the Bragg reflections for perfectly ordered crystals. Hence this component is fully coherent in the latter case. This scattering channel can be completely eliminated except forward direction provided the incoming parallel beam is fairly monochromatic and the scattering target is made of a single crystal set out of the Bragg conditions. On the other hand, any kind of disorder leading to the partly stochastic occupation of various perfect sub-lattices within the single crystal by atoms having distinctly different cross-sections for the Rayleigh scattering leads to the presence of the incoherent and elastic component in the scattered radiation. This component is emitted in all directions from the illuminated spot and it is super-imposed on the incoherent inelastic component, Compton component and X-ray fluorescence component. Multiple Compton scattering is usually negligible for typical X-ray energies of the incoming radiation. There is no distinction between Compton and Rayleigh components in the vicinity of the forward direction. A parallel and almost monochromatic incoming beam has to make some sufficiently large angle with the sample surface to avoid grazing angle scattering. A correction due to the sample refractive index usually can be neglected at the typical incoming photon energies and for sufficiently large scattering angles. The incoherent and elastic component could be partly or fully converted into the quasi-elastic incoherent component due to the atomic jumps within or between various Bravais sub-lattices. The last process is the point of interest of this paper for samples being globally and locally in a thermal equilibrium [12].

Let us consider a single crystal composed of $S \geq 1$ perfect primitive Bravais sub-lattices occupied by $M \geq 1$ different kind of atoms including mono-vacancies. Here different kind of atoms are in fact atoms of distinctly different elements. In such a case one can assume that interstitial atoms are absent. It is assumed additionally that the crystal remains in a thermal equilibrium and that particular atoms including mono-vacancies are stochastically distributed in each sub-lattice. Atoms and mono-vacancies are supposed to execute independent thermal vibrations around respective equilibrium positions. It is assumed that the first Born approximation applies as long as the Rayleigh scattering is considered. The last assumption is valid even for the infinitely thick samples due to the large cross-sections for the photo-effect in the typical X-ray energy range. Let the index $s = 1,2,...,S$ enumerates different sub-lattices, while the index $m = 1,2,...,M$ different kind of atoms including mono-vacancies. In such a case a probability $p_{ms} \geq 0$ to find the atom of the $m-th$ kind in any vertex of the $s-th$ sub-lattice satisfies the relationship $\sum_{m=1}^{M} p_{ms} = 1$, as "something" has to be found in each vertex. On the other hand, the Rayleigh scattering amplitude could be expressed as $F_{ms}(\mathbf{q}_0\mathbf{q} \mid \boldsymbol{\varepsilon})$ for the $m-th$ kind of atom located in the $s-th$ sub-lattice. Here the symbol $\mathbf{q}_0$ denotes a wave-vector of the incoming monochromatic radiation, while the symbol $\mathbf{q}$ stands for the wave-vector transfer to the sample during the elastic scattering. Finally the symbol $\boldsymbol{\varepsilon}$ denotes a unit vector perpendicular to the wave-vector of the incoming radiation and lying within the polarisation plane of the incoming radiation, i.e., within the plane of the electric field vector. The Rayleigh scattering has predominantly E1 character for typical X-ray energies and therefore it is practical to use linearly polarised incoming radiation with the polarisation plane being perpendicular to the scattering plane. In such a case the scattered radiation has the maximum possible intensity particularly for the scattering angle being close to the right angle. The average scattering amplitude by the vertex s can be expressed as:

$$\alpha_s = \sum_{m=1}^{M} p_{ms} F_{ms}(\mathbf{q}_0\mathbf{q} \mid \boldsymbol{\varepsilon}). \tag{1.1}$$

One has to note that all vortices of the particular sub-lattice are equivalent. On the other hand, particular average incoherent scattering amplitude by the $m-th$ kind of atom located in the $s-th$ vertex can be calculated as:

$$a_{ms} = \sqrt{\frac{p_{ms}}{M(1-p_{ms})}}\,[F_{ms}(\mathbf{q}_0\mathbf{q} \mid \boldsymbol{\varepsilon}) - \alpha_s]. \tag{1.2}$$

It has to be noticed that the above amplitude vanishes for p_{ms} being either zero or unity, i.e., for a perfectly ordered sub-lattice including completely empty sub-lattices. Hence the scattering amplitude by the mono-vacancy can be approximated as $F_{ms}(\mathbf{q}_0\mathbf{q} \mid \boldsymbol{\varepsilon}) = 0$. A total incoherent scattering cross-section per single chemical unit cell amounts to:

$$\sigma_0 = \sum_{m=1}^{M} \sum_{s=1}^{S} a_{ms} a_{ms}^{*}. \tag{1.3}$$

A corresponding cross-section for the elastic scattering can be calculated according to the expression:

$$\sigma = \sum_{m=1}^{M}\sum_{s=1}^{S} a_{ms} a_{ms}^{*} f_{ms}(\mathbf{q}) .$$

(1.4)

Here the symbol $0 \le f_{ms}(\mathbf{q}) \le 1$ denotes respective recoilless fraction being dependent upon the wave-vector transfer to the crystal. A recoilless fraction of the mono-vacancy can be calculated as [12]:

$$f_{\nu s}(\mathbf{q}) = \frac{\sum_{m \neq \nu} p_{ms} f_{ms}(\mathbf{q})}{\sum_{m \neq \nu} p_{ms}} .$$

(1.5)

Here the symbol ν denotes a mono-vacancy. The expression (1.4) gives a complete description of the incoherent elastic scattering process as long as atoms remain in the vicinity of the equilibrium positions. However atomic jumps between and within sub-lattices lead to the quasi-elastic processes. One can assume that the latter processes do not exchange energy between the beam and the sample on the average as long as the sample remains in the equilibrium – usually one can neglect sample heating by the beam. Hence one has to introduce a scattering function by the average chemical unit cell. This scattering function is a function of the correlation time $t \ge 0$, and it takes on the following general form:

$$S(t) = \sum_{m=1}^{M}\sum_{m'=1}^{M} \sigma_{mm'} \sum_{s=1}^{S}\sum_{s'=1}^{S}\sum_{\lambda} V_{\lambda ms} U_{m's'\lambda} \exp(\lambda t) .$$

(1.6)

Here the cross-section $\sigma_{mm'}$ is a partial elastic incoherent cross-section for scattering by the atom of the $m-th$ kind and it takes on the following form:

$$\sigma_{mm'} = \delta_{mm'} \sum_{s=1}^{S} a_{ms} a_{m's}^{*} \sqrt{f_{ms}(\mathbf{q}) f_{m's}(\mathbf{q})} .$$

(1.7)

One has to note that the last expression is diagonal in the indices m as atoms and vacancies are conserved in the diffusion processes. Symbols $V_{\lambda ms}$ and $U_{m's'\lambda}$ denote elements of the left and right eigenvectors of the diffusion operator, respectively, while the symbol $\lambda \le 0$ stands for the corresponding eigenvalue of the above operator. Due to the fact that the detection systems are unable to separate elastic and inelastic components of the Rayleigh scattered radiation it is convenient to introduce the following correlation function $G(t) = f_0[S(t)/S(0)]$ with $f_0 = \sigma / \sigma_0$ being an effective recoilless fraction [12]. It has to be noted that processes involving phonon creation or annihilation lead to the almost immediate loss of correlation as the energies exchanged are quite large. On the other hand, it has to be noted that for the Bragg conditions being satisfied the scattering function satisfies the following condition $S(t)/S(0) \equiv 1$. The last statement applies to the forward scattering as well.

One can ask about the mixed terms between different kind of atoms in the case of correlated jumps. Particularly each vacancy jump is associated with the respective atomic jump in the opposite direction. However it has to be remembered that the Rayleigh scattering volume of the single photon encompasses very large number of atoms in the condensed phase. In such a case the mixed terms are averaged out even for highly ordered samples.

A scattering function described by the equation (1.6) can be easily transformed into the frequency domain ω applying the Fourier transformation. Such a transformation leads to the following expression [12]:

$$S(\omega) = (2\pi)^{-1} \int_0^{\infty} dt\, S(t) [e^{i\omega t} + e^{-i\omega t}] = \pi^{-1} \sum_{m=1}^{M} \sum_{m'=1}^{M} \sigma_{mm'} \sum_{s=1}^{S} \sum_{s'=1}^{S} \sum_{\lambda} V_{\lambda ms} U_{m's'\lambda} \left[(-\lambda) / (\lambda^2 + \omega^2) \right]. \tag{1.8}$$

Usually one has to normalise the above function in such a way to get the following correlation function in the frequency domain $G(\omega) = N_0^{-1} S(\omega)$, where the normalisation constant is defined as $N_0 = \int_{-\infty}^{\infty} d\omega\, S(\omega)$. It has to be stressed that the correlation functions $G(t)$ and $f_0 G(\omega)$ contain exactly the same physical information about the underlying dynamics. In particular the correlation function obeys the equation $G(\omega) = \delta(\omega)$ either in the forward or Bragg direction.

1.1. DIFFUSION OPERATOR

A diffusion operator [13-17] is diagonal in the indices m due to the fact that types of atoms are conserved during jumps. One can assume that diffusion in a crystalline material proceeds via jumps between adjacent vortices of various sub-lattices with relatively long residence times between subsequent jumps [18-22]. In the case of highly disordered systems considered here, each jump constitutes a diffusion event uncorrelated to the previous and subsequent events. Duration of the diffusion event is very short. In such a case diagonal elements of the diffusion operator take on the form:

$$W_{ss}^{(mm')} = -\delta_{mm'} \{ \omega_s^{(m)} [1 - \alpha_s^{(m)}(\mathbf{q})] + \sum_{s' \neq s} \omega_{ss'}^{(m)} \}. \tag{1.9}$$

Here the symbol $\omega_s^{(m)} \geq 0$ stands for the average jump rate of the $m-th$ kind of atom. These particular jumps originate at any vertex of the $s-th$ sub-lattice and lead into any another vertex of the same sub-lattice. The symbol $\alpha_s^{(m)}(\mathbf{q})$ denotes corresponding geometrical factor for the above jump. A jump rate $\omega_{ss'}^{(m)} \geq 0$ describes jumps of the $m-th$ kind of atom originating in any vertex of the $s-th$ sub-lattice and ending in any vertex of the different sub-lattice enumerated by the index s'. Off diagonal elements of the diffusion operator can be expressed as:

$$W_{ss'}^{(mm')} = \delta_{mm'} \omega_{ss'}^{(m)} \alpha_{ss'}^{(m)}(\mathbf{q}) \text{ for } s' > s \text{ and } W_{s's}^{(m)} = \delta_{mm'} (p_{ms} / p_{ms'}) \omega_{ss'}^{(m)} [\alpha_{ss'}^{(m)}(\mathbf{q})]^*. \tag{1.10}$$

The last expression is valid for the sample being locally at the thermal equilibrium [23,24]. The symbol $\alpha_{ss'}^{(m)}(\mathbf{q})$ denotes a geometrical factor for a jump between various sub-lattices.

Geometrical factors can be calculated according to the expressions:

$$\alpha_s^{(m)}(\mathbf{q}) = \sum_n W_n^{(ms)} \cos(\mathbf{q} \bullet \mathbf{r}_{sn}) \text{ and } \alpha_{ss'}^{(m)}(\mathbf{q}) = \sum_n W_n^{(mss')} \exp[i(\mathbf{q} \bullet \mathbf{r}_{ss'n})]. \tag{1.11}$$

The symbol $W_n^{(ms)} \geq 0$ stands for a probability to reach the vertex n of the $s-th$ sub-lattice by the $m-th$ kind of atom starting from another vertex of the same sub-lattice. The index n is relative and it refers to the vertex of the origin of the jump. Similarly the symbol $W_n^{(mss')} \geq 0$ denotes a corresponding probability for a jump to a different sub-lattice. Hence the above probabilities are normalised as follows $\sum_n W_n^{(ms)} = 1$ and $\sum_n W_n^{(mss')} = 1$. Symbols $\mathbf{r}_{sn}$ and $\mathbf{r}_{ss'n}$ denote respective non-zero jump vectors originating at the vertex of the origin of the jump and pointing into vertex where the atom concludes its jump.

Some additional constrains apply to the occupation probabilities due to the fact that the composition of the crystal remains constant at equilibrium. Namely, these constrains can be expressed as:

$$\frac{\sum_{s=1}^{S} p_{ms}}{\sum_{s=1}^{S} p_{m's}} = x_{mm'} \text{ for } m' \neq m . \tag{1.12}$$

Here the symbol $x_{mm'}$ denotes the ratio of the concentrations of the $m-th$ kind of atoms and the $m'-th$ kind of atoms, respectively.

A diffusion operator satisfies the eigen equation $\mathbf{VWU} = \boldsymbol{\lambda}$ with $\mathbf{VU} = \mathbf{UV} = \mathbf{1}$, where the symbols $\mathbf{V}$ and $\mathbf{U}$ stand for the left and right eigenvector matrices, respectively, while the symbol $\boldsymbol{\lambda}$ denotes a diagonal matrix of real eigenvalues being not greater than zero. The symbol $\mathbf{1}$ denotes a unit matrix. The above matrices have dimensions [MS x MS]. The left eigenvectors constitute rows of the matrix $\mathbf{V}$, while the right eigenvectors constitute columns of the matrix $\mathbf{U}$.

The above formalism allows calculation of a diffusion coefficient tensor for each kind of atoms according to the relationship:

$$\mathbf{D}_m = \frac{\sum_{s=1}^{S} p_{ms} \left(\omega_s^{(m)} \sum_n W_n^{(ms)} (\mathbf{r}_{sn} \otimes \mathbf{r}_{sn}) + \sum_{s' \neq s} \omega_{ss'}^{(m)} \sum_n W_n^{(mss')} (\mathbf{r}_{ss'n} \otimes \mathbf{r}_{ss'n}) \right)}{\sum_{s=1}^{S} p_{ms}} . \tag{1.13}$$

The latter tensors are symmetrical real tensors of the second order in a three dimensional configuration space. Diagonal elements of these tensors are non-negative.

1.2. SCATTERING AMPLITUDES

Usually one can assume that the scattering amplitude of the particular atom is independent of the sub-lattice, i.e., one can assume that the relationship $F_{ms}(\mathbf{q}_0\mathbf{q} \mid \boldsymbol{\varepsilon}) = F_m(\mathbf{q}_0\mathbf{q} \mid \boldsymbol{\varepsilon})$ is well satisfied. Furthermore the latter amplitude could be factorised into polarisation independent and polarisation dependent parts in the following manner provided a scattering is of the dipolar character:

$$F_m(\mathbf{q}_0\mathbf{q}\,|\,\boldsymbol{\varepsilon}) = F_m(\mathbf{q}_0\mathbf{q})\sqrt{1-[\sin(\theta)\sin(\beta)]^2}\ .$$

(1.14)

A polarisation dependent part is independent of the scattering atom as long as the scattering is of the E1 character and the scattering is indeed of this character for typical X-ray energies. Here the angle $0 \le \theta \le \pi$ is the scattering angle, while the angle $0 \le \beta \le \pi/2$ is the angle between the unit vector perpendicular to the scattering plane and the unit vector $\boldsymbol{\varepsilon}$. The latter angle could be calculated according to the relationship:

$$\beta = a\cos\left(\sqrt{\frac{\{[\mathbf{q}_0\times(\mathbf{q}_0-\mathbf{q})]\bullet\boldsymbol{\varepsilon}\}^2}{[\mathbf{q}_0\times(\mathbf{q}_0-\mathbf{q})]\bullet[\mathbf{q}_0\times(\mathbf{q}_0-\mathbf{q})]}}\right).$$

(1.15)

The polarisation dependent part equals unity provided the latter angle equals zero, i.e., for the case of mutually orthogonal scattering and polarisation planes. In such a case the scattering amplitude reaches the maximum in absolute terms.

A polarisation independent part of the amplitude depends mainly upon the wave functions of the core electrons. Therefore it can be approximated by the expression $F_m(\mathbf{q}_0\mathbf{q}) = F_m(q_0\theta)$, where the symbol $q_0 > 0$ denotes the wave number of the incident radiation to the sufficient accuracy. The latter amplitude can be calculated according to the relationship:

$$F_m(q_0\theta) = \sqrt{\frac{8\pi}{3}}\left(\frac{\mathrm{e}^2}{\mathrm{m}_0\mathrm{c}^2}\right)[\eta_m(q_0\theta) + i\chi_m(q_0)].$$

(1.16)

Here the symbol e denotes the elementary charge, m_0 stands for the rest mass of the free electron and c denotes the velocity of light in vacuum. The real part of the amplitude $\eta_m(q_0\theta)$ depends on the scattering angle due to the fact that the size of the electron shell is comparable to the wavelength of the scattered radiation, while the imaginary part $\chi_m(q_0)$ is independent of the scattering angle. The latter part becomes significant close to the absorption edges as it is strongly correlated with the cross-section for the photo absorption. Both of the above parameters could be calculated applying relativistic atomic Hartree-Fock electron wave functions. One has to note that the amplitude $\eta_m(q_0\theta)$ equals Z_m in the forward direction, where all the partial waves are fully coherent, i.e., in phase. Here Z_m denotes the atomic number of the scattering atom or ion. Hence heavy atoms are privileged as the scattering centres and sufficient contrast could be achieved for atoms differing significantly in atomic numbers. Finally, it is worth to mention that the wave number transfer to the sample satisfies the following relationship for a single scattering process of the almost elastic character $q = 2q_0\sin(\theta/2)$.

2. EXPERIMENTAL METHODS

The fullest information can be gained applying microscopic methods sensitive to the wave-vector and energy transfer. Single crystalline samples allow to control over the direction of wave-vector transfer, while the scattering methods allow to control additionally the wave number transfer. In order to get spatial resolution on the atomic scale one has to apply significant wave number transfers, and hence one has to resort to either X-ray or neutron

scattering [18,19,25]. It is desirable to have a method sensitive to the wide range of elements as well. Diffusive motions in solids are rather slow, and therefore a very good energy resolution is required.

There are few methods being able to satisfy all of the above conditions. One can mention a quasi-elastic incoherent neutron scattering (QNS) or neutron spin echo spectroscopy (NSE). The energy resolution of QNS is barely sufficient and thus this method is applicable to samples exhibiting a very fast diffusion. The energy resolution of NSE can be very good, but at the very small wave number transfers. One has to note that the wave number accessible by QNS is small as well. Usually one cannot encompass any non-trivial reciprocal lattice point especially for small unit cells [18,26].

A photon correlation spectroscopy (PCS) seems a great hope, but at the present state of the art it is unable to reach the spatial resolution at the atomic scale. It is believed that such a resolution would be achieved applying free electron lasers operating in the X-ray region. It has to be realised that PCS has intrinsically very large time window, and hence it is suitable to look upon extremely slow processes. It is useless for a bit faster processes [27,28].

Another possibility is to use a resonant X-ray interferometry discussed in detail here. This method was applied successfully to glasses, [8], and it has obvious future as far as the disordered crystalline matter discussed above is considered. Single crystals are the best choice. It has to be mentioned that relatively small samples are required, what makes easier to produce suitable single crystals. This method is characterised by a very good spatial resolution and fairly good energy resolution provided a proper nuclear transition is chosen.

All of the above methods can operate either in the frequency (energy) domain or in the time domain depending upon the particular method. Methods operating in the energy domain look at the following function in a more or less direct way:

$$P(\omega) = \int_{-\infty}^{\infty} d\omega' \, D(\omega - \omega') \int_{-\infty}^{\infty} d\omega'' \, A(\omega'') \, G(\omega' - \omega'') \,. \tag{2.1}$$

Here the function $A(\omega)$ represents emission profile of the radiation source, while the function $D(\omega)$ represents a resolution function of the scattered radiation detector. The simplest such method is based upon Rayleigh scattering of the Mössbauer radiation (RSMR). Unfortunately resonant sources emitting sufficiently narrow lines are too weak to apply successfully and routinely RSMR for diffusion research in single crystals [29-31]. The main drawback is due to the isotropic emission of the radiation from the radioactive source. This obstacle is removed while applying synchrotron radiation (SR) as beams coming out of the undulator are almost parallel. Hence the nuclear resonant targets inserted in such beams can replace traditional Mössbauer sources and absorbers. Pulsed SR beams allow to separate enormous prompt pulse from the weak delayed and resonant radiation. Hence the latter method is a typical time domain method.

2.1. RADIATION SOURCES AND X-RAY OPTICS

Undulators mounted on the electron or positron storage rings are the sole sources of radiation suitable for the purpose nowadays. They are to be replaced soon by the free electron lasers once the latter devices are able to reach sufficient X-ray energy. A storage ring has to be

operated in the pulse mode with a single bunch or multiple bunches equally separated in time. It is desired to have structure-less pulse of the very short duration. The energy of the electrons or positrons has to be of the order of several GeV. Undulators producing linearly polarised light are preferred. Radiation coming out of such a device has the following basic properties:

1. the energy spectrum has a single broad maximum of about 1.5 keV centred around the desired energy, the latter being variable from about several keV till about 100 keV
2. the beam is composed of short pulses of about several ps duration each
3. pulses appear equally spaced in time with a time period between adjacent pulses varying from less than 200 ns till almost 3000 ns depending upon the storage ring and number of bunches circulating within it
4. radiation is almost perfectly linearly polarised and the orientation of the polarisation plane can be varied in principle
5. the beam is almost parallel in both mutually orthogonal directions perpendicular to the direction of propagation
6. the cross-section of the beam is fairly homogeneous, remains stable in the space and amounts typically to about 0.5 x 2.5 mm

A multiple stage single crystal monochromator has to be inserted into the beam just beyond the undulator in order to cut out a bandwidth of about 100 meV around the desired energy. Such a device is essential to reduce the overload of the detector at the prompt pulse [4-6].

It is desirable to reduce the cross-section of the beam several times in both directions perpendicular to the direction of propagation. A simple slit leads to the serious loss of the intensity. Hence some focusing device has to be applied in such a way to preserve the beam parallelism. One can apply two conical Fresnel lenses, but it is very difficult to make efficient lenses in the energy range of the beam photons. It is proposed here to use a device shown in the Fig. 1.

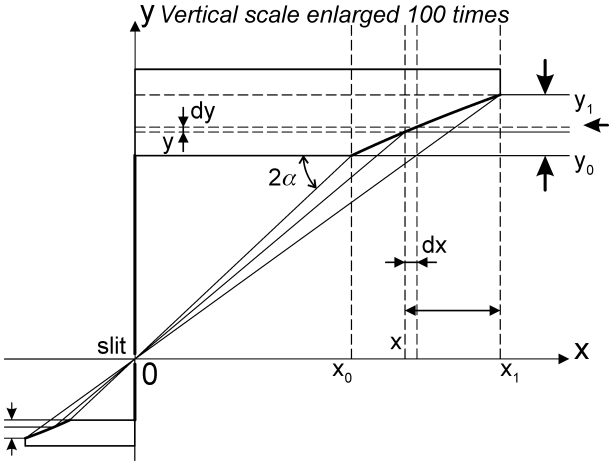

Fig. 1 Basic principle of the proposed beam concentrator

The beam propagates in the direction $-x$ and it is contained within the range $0 < y_0 < y_1$ with the direction y being perpendicular to the direction x. The ray passing through the point $\{x_0, y_0\}$ is scattered at this point into the focus located at the origin. A very thin grazing incidence mirror is used to scatter the beam. A scattering angle is denoted as $\phi = 2\alpha$ with the angle α being lesser than the grazing angle at each point of the mirror. Once the angle α and

the co-ordinate y_0 are chosen one can calculate the remaining co-ordinate of the point $\{x_0, y_0\}$ according to the expression $x_0 = y_0\, tan^{-1}(2\alpha)$. Subsequently one can choose the increment of the co-ordinate y satisfying the expression $dy << y_1 - y_0$, where $y_1 - y_0$ stands for the incoming beam width. Furthermore one can proceed iteratively applying subsequently the following set of equations: $dx = dy/tan(\phi), x = x + dx, y = y + dy$ and $\phi = atan(y/x)$ until the co-ordinate y exceeds the maximum required value y_1, where the co-ordinate x exceeds the value of the co-ordinate x_1. Hence one obtains all co-ordinates $\{x, y\}$ of the mirror surface satisfying the required condition to focus all rays in the origin. The mirror is flat in the third dimension perpendicular to x and y axes both. It has to intercept the whole beam in this direction, of course. The point y_0 has to be chosen somewhat below the lower edge of the beam. One can consider the front wave as undistorted till the scattering point having co-ordinate x. On the other hand, a distance travelled from that point till the focus can be calculated as $R = x_1 - x + \sqrt{x^2 + y^2}$. These distances do not differ significantly while calculated for various scattering points due to the very long focal length of the device enforced by the necessity to keep scattering angles within the grazing incidence limits. Hence the pulse is not smeared significantly on the time scale upon having applied this device. The beam parallelism can be restored applying inversion of the above device around the focus and scaling down dimensions x and y. Some slit has to be mounted in the vicinity of the focus. Hence a complete device is composed of two mirrors arranged around the focal line perpendicular to x and y directions both. Concentrated beam comes out as parallel to the original beam albeit it is displaced in the $-y$ direction. Two such devices applied in series are able to concentrate the beam in both directions perpendicular to the direction of propagation provided their focal lines are mutually orthogonal. It is desirable to place them in vacuum. A mirror surface has to be made of some heavy element e.g. gold. Devices described above are completely reversible. Hence they can be used as beam expanders as well provided the direction of propagation is reversed. The above devices are broad band devices and their properties do not depend upon the photon energy within the bandwidth of the single crystal monochromator mounted up the beam.

Subsequently the beam has to pass the interferometer containing the sample investigated. The interferometer is described in the following sub-section. It is desirable to have beam monitors just prior to entering the interferometer and just before reaching a detector slit. The best monitors are thin foils made of the light element like beryllium, oriented at some angle to the beam direction and scattering a tiny fraction of radiation (mainly at the prompt pulse) into some solid state detectors. A scattering within monitors proceeds mainly via the Compton mechanism.

The beam is scattered by the sample investigated in all directions and the scattered radiation contains unwanted fluorescent and Compton components. Hence it is important to remove these components from the radiation reaching the detector. One has to note that the detectors being able to recover very fast after the prompt pulse and having very good time resolution are characterised by poor energy resolution. Usually avalanche photo-diodes (APD) are used as detectors of radiation [32]. It is proposed to apply for this purpose a curved Bragg mirror inserted beyond the resonant targets. It has to be inserted beyond the interferometric part as it produces some coherent inelastic component. The basic arrangement of such a monochromator is shown in the Fig. 2.

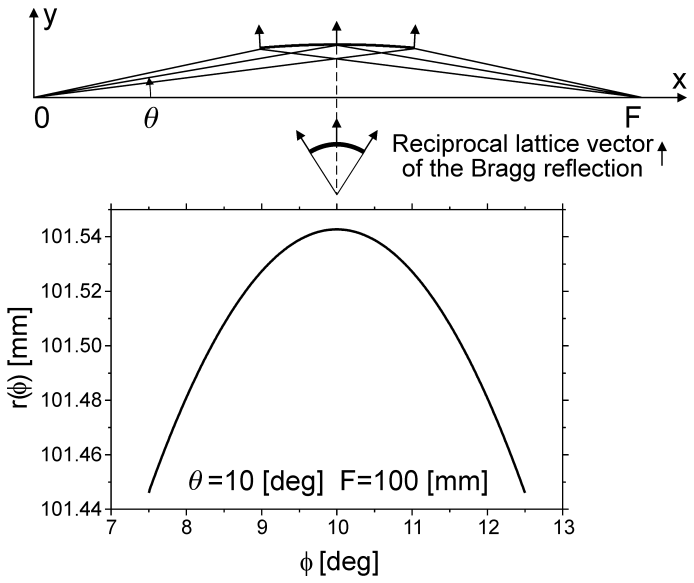

Fig. 2 Bragg mirror proposed to remove fluorescent and Compton components

The mirror is able to remove fluorescent component and the Compton component provided the latter is not produced at very small scattering angles. However, it has insufficient resolution to remove the Rayleigh incoherent inelastic component originating in the sample investigated. The mirror defines the range of the scattering angles accepted by the detector as well. Let the illuminated spot on the sample surface be located at the origin and the mirror focus somewhere on the positive part of the x axis in the distance F from the origin. The x axis is a rotation symmetry axis of some curved and closed surface having additionally a symmetry plane perpendicular to the x axis and located half way between the origin and the focus. A mirror is a part of this surface chosen in such a way that the above mentioned plane is a symmetry plane of the mirror as well, and additionally the $[x, y]$ plane is another symmetry plane of the mirror. All points belonging to the mirror have positive co-ordinates y. The mirror dimension along the x axis is much smaller than the focal distance F. The inner surface of the mirror has to be covered by a thin single crystal oriented at each point of the mirror in such a way to satisfy Bragg conditions for a chosen Bragg reflection and photons of the desired energy. All these photons come from the origin and they have to be scattered into the focus. It is sufficient to arrange the single crystal in such a way to have a reciprocal lattice vector of the desired Bragg reflection perpendicular to the crystal surface at each point of the mirror surface. Let us denote by the symbol ϕ the angle between the x axis and a particular ray coming out of the origin. In such case co-ordinates of the mirror point lying in the $[x, y]$ plane can be expressed as follows:

$$x = [F\ tan(\theta - \chi)]/[tan(\theta + \chi) + tan(\theta - \chi)],\ \ y = tan(\theta + \chi) \text{ and } \chi = \phi - \theta . \tag{2.2}$$

Here the angle θ stands for the Bragg angle satisfying the following condition for the scattering angle of the mirror $0 < 2\theta < \pi/2$. Co-ordinates of the above curve have to satisfy the following conditions $0 < x < F$ and $y > 0$. A differential angle χ has to satisfy the condition $|\chi| << \theta$, while the Bragg angle have to be rather small. It is desirable to use strong Bragg reflections for the purpose. One can calculate a curve for some range of the co-ordinates x (it has to be calculated symmetrically around the plane perpendicular to the x axis and located half way between the origin and the focus). The latter curve can be rotated

symmetrically by some right and left handed small angle around the x axis. Hence a complete surface of the mirror can be defined. A detector slit has to be located in the vicinity of the focus. It is desirable to place a beam monitor between the mirror and the detector slit. It is assumed that the mirror is located in the vacuum. It is impossible to satisfy simultaneously equal path condition for all rays going from the origin to the focus and Bragg conditions at each point of the mirror, as the latter condition leads to the non-ellipsoidal surface of the mirror. A distance travelled depends upon the angle ϕ in the following way:

$$r(\phi) = \sqrt{x^2(\phi) + y^2(\phi)} + \sqrt{[F - x(\phi)]^2 + y^2(\phi)} \ . \tag{2.3}$$

The inset of the Fig. 2 shows this distance for a range of the angles ϕ centred around the Bragg angle $\theta = 10^o$ (scattering angle $2\theta = 20^o$) and for the focal length chosen as $F = 100\,\mathrm{mm}$. It is obvious that under such conditions the loss of the time resolution is negligible.

2.2. RESONANT X-RAY INTERFEROMETER

Resonant X-ray interferometers have been already applied to the amorphous targets and described from a theoretical point of view in the literature [8,9]. A theory presented here is based on a more general and compact formalism based on the use of the density-like matrices.

A homogeneous locally flat target containing resonant nuclei emitting single line of the natural width has the following response function for the nuclear forward scattering [9]:

$$\psi_n(x) = \tfrac{1}{2}\left(L_n / x\right)^{1/2} J_1\left(\left[L_n x\right]^{1/2}\right) \exp\left(\left[-\tfrac{1}{2} + i\omega_n\right] x\right) . \tag{2.4}$$

The above expression is valid provided the saturation effects are negligible. Here the symbol $x = \gamma t$ denotes a reduced time with the symbol γ denoting natural width of the resonant line and the symbol t standing for a time interval elapsed from the prompt pulse. The parameter $L_n = \mu_n^{(R)} z_n (1 + i\xi)$ describes a target thickness for the resonant absorption [33]. Here the symbol $\mu_n^{(R)}$ denotes a resonant absorption coefficient of the target material, z_n stands for the target thickness along the beam path and ξ stands for the coefficient describing interference between nuclear processes and atomic processes coherent with the previous processes. A photo-effect is coherent with the nuclear absorption followed by the internal conversion, while the Rayleigh scattering is partly coherent with the nuclear photon reemission. It is worth mentioning that for pure M1 nuclear transitions the interference coefficient is negligible as the photo-effect and Rayleigh scattering are predominantly of the E1 character and these two amplitudes are mutually orthogonal each other. The symbol ω_n stands for the resonant frequency of the target, while the index $n = 1,2$ enumerates targets. Finally the symbol J_1 denotes a Bessel function of the first order and kind.

The best choice is to use identical targets kept at the same temperature. One of them has to be a flat foil located between the beam concentrator and the sample investigated, while the other one has to be a part of the sphere centred on the illuminated spot of the sample and located between the sample and the Bragg mirror. Both targets are locally perpendicular to the beam. Due to the fact that absolute resonant frequencies are not directly observable one can set the following conditions for identical targets: $\omega_1 = (q_0 v)/\gamma$ and $\omega_2 = 0$. Here the index $n = 1$

refers to the first target located up the beam, while the index $n = 2$ refers to the remaining target. The resonant energy difference between targets can be generated applying the first order Doppler shift between them. Basically one can make movable either the first or the second target. Even the non-resonant Rayleigh scattering sample can be made movable [34]. It is practical to move the first target along the beam with the constant velocity v. Due to the fact that the amplitude of such a motion is limited one has to reverse the velocity several times per second keeping the same absolute value for the forward and backward motions. The sign of the velocity has no influence on the data as long as the correlation functions are purely real, i.e., in the case of the diffusion. Hence the movable target executes a periodic motion having very small displacement amplitude around some constant and predefined average position. Mössbauer transducers of the latest generation are able to perform this task in the excellent manner. They are equipped with the hollow central tube in order to pass the beam [35].

Generally there are four interfering amplitudes involved: the prompt signal separated from the delayed signals on the time scale, the amplitude due to the first target, the amplitude due to the second target down the beam and the interaction amplitude between the first and the second target. The last amplitude vanishes provided a high velocity between targets is applied. Hence a total amplitude can be written as a ket in the four dimensional space:

$$|\phi> = \begin{bmatrix} P \\ \psi_1(x) \\ \psi_2(x) \\ -\int_0^x dx' \psi_1(x') \psi_2(x-x') G(x') \end{bmatrix}. \tag{2.5}$$

Here the symbol P stands for the prompt amplitude. One has to note that the correlation function $G(x) = 1$ in the absence of the scattering sample and for such an arrangement that the beam passes both targets in a series.

The intensity of the radiation on the detector can be calculated versus reduced time as $I(x) = C < \phi | \mathbf{T} | \phi >$, where the constant $C > 0$ stands for the irrelevant normalisation constant. Usually one can adopt this constant in such a way to obtain $I(0) = 1$, i.e., $C = \left(< \phi | \mathbf{T} | \phi > \right)_{x=0}^{-1}$. A density-like operator $\mathbf{T}$ takes on the following form:

$$\mathbf{T} = \begin{bmatrix} \delta(x) & 0 & 0 & 0 \\ 0 & 1 & G(x) & G(x) \\ 0 & G^*(x) & 1 & 1 \\ 0 & G^*(x) & 1 & 1 \end{bmatrix}. \tag{2.6}$$

One has to note that the detector has to be blocked just before the prompt pulse and opened some time t_0 after the prompt pulse upon having recovered from the shock of the prompt pulse. A detector recovery time takes on usually several ns. A detector has to be blocked during reversing of the velocity sign as well. A detector background is negligible for properly designed radiation source, beam path and for a proper setting of the discrimination levels of the electronics counting detected photons. A time resolution of the detector can be made as good as about 100 ps in the long term. Hence data can be collected versus time scale having

origin at the prompt pulse in the equal duration adjacent time channels having width Δt of the order of the time resolution. Very early data channels remain empty due to the necessity to recover the detector. The total number of the data channels N_c is about 10^3.

The above formalism is linear as long as the fourth component of the amplitude is negligible. Otherwise this component introduces some non-linearity. The operator described by the expression (2.6) is Hermitean.

Some modification is essential provided the separation of adjacent pulses is shorter than the complete decay time of the excitations in the resonant targets. One can assume that the system remains in some long-term equilibrium as the average intensity of the radiation coming out of the undulator evolves very slowly with time. In such a case one can define the following response functions:

$$\psi_1^{(m)}(x) = \psi_1(x + mx_0) \text{ and } \psi_2^{(m)}(x) = \psi_2(x + mx_0). \tag{2.7}$$

Here the index $m = 0,1,2,...$ enumerates the past prompt pulses. The most recent pulse has the number $m = 0$. On the other hand, the parameter x_0 can be expressed as γT_R, where the symbol T_R stands for the time interval between adjacent pulses (they are equally spaced in time). Hence one can define partial amplitudes in the ket form according to the relationship:

$$|\phi_m> = \begin{bmatrix} P \\ \psi_1^{(m)}(x) \\ \psi_2^{(m)}(x) \\ -\int_{-mx_0}^{x} dx' \psi_1(x'+mx_0)\,\psi_2(x-x')\,G(x'+mx_0) \end{bmatrix}. \tag{2.8}$$

Subsequently one can define a partial density-like operator in the form:

$$\mathbf{T}_{lm} = \begin{bmatrix} \delta_{lm}\delta(x-mx_0) & 0 & 0 & 0 \\ 0 & 1 & G(x+lx_0) & G(x+lx_0) \\ 0 & G^*(x+mx_0) & 1 & 1 \\ 0 & G^*(x+mx_0) & 1 & 1 \end{bmatrix}. \tag{2.9}$$

Finally one can calculate a modified intensity according to the relationship:

$$I_M(x) = C_M \sum_{m=0}^{\infty}\sum_{l=0}^{\infty} <\phi_l | \mathbf{T}_{lm} | \phi_m> \text{ with } C_M = \left(\sum_{m=0}^{\infty}\sum_{l=0}^{\infty} <\phi_l | \mathbf{T}_{lm} | \phi_m> \right)^{-1}_{x=0}. \tag{2.10}$$

One has to note that the following general rules are satisfied for the response functions and the correlation function: $\psi_1(x<0) = \psi_2(x<0) = G(x<0) = 0$. It has to be noted that the operator (2.9) is not necessarily Hermitean for the most general cases. However the following linear combinations $\mathbf{T}_{lm} + \mathbf{T}_{ml}$ are always Hermitean, and hence the calculated intensity is always real and non-negative as in the previous simplified formalism. The series of the

equation (2.10) is very fast convergent. It is assumed here that the beam modifies neither the target nor the sample properties.

A complete device beyond the beam concentrator is shown schematically in the Fig. 3. One can use simultaneously several detection channels containing its own second targets and Bragg mirrors in order to measure data simultaneously at various wave-vector transfers. It is practical to arrange them in a plane perpendicular to the polarisation plane of the incoming beam. A scattering geometry is more useful than the transmission geometry as far as the sample positioning is concerned as the previous geometry allows using thick samples. Such samples are more stable at the high temperatures required to obtain fast enough diffusion.

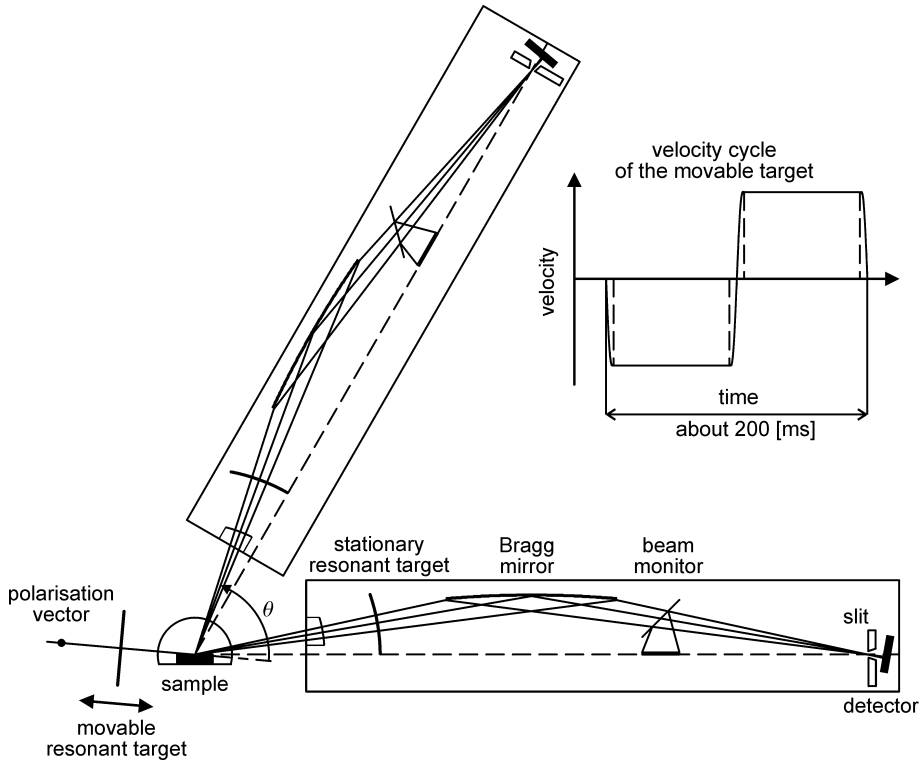

Fig. 3 Schematic view of the resonant X-ray interferometer
The angle θ is a good approximation to the scattering angle for relatively small acceptance solid angle of the Bragg mirror.

The best resonant line available is the 14.41 keV line connecting ground state of the stable ^{57}Fe nucleus with its first excited state having lifetime $\tau = 1/\gamma = 141\,\mathrm{ns}$. It is practically purely M1 transition and therefore the parameter $\xi = 0$ [36]. The wave number of this line is equal $q_0 = 73\,\mathrm{nm}^{-1}$, and hence wave number transfers up to about to 140 nm^{-1} can be achieved assuring a very good spatial resolution. The energy resolution can be as good as $1\,\mathrm{neV}$ provided relatively thin targets are applied and the adjacent pulse separation exceeds about 200 ns. Very strong radiation sources are necessary to reach this limit. On the other hand, the maximum bandwidth still detectable has to stay within the limit of about 100 neV. One can extend the above limit by about an order of magnitude using stationary both resonant targets and relying upon the intensity due to the fourth component of the ket amplitude [9]. In that case thick resonant targets are desirable. However the latter method is less precise than the application of the moving target. The optimum velocity of the moving target is about $\pm 3\,\mathrm{mm/s}$. The best targets can be made of polycrystalline rhodium foils having thickness of

several μm with the several at. % of ^{57}Fe alloyed homogeneously in. Such targets can be kept in the temperature close to the room temperature. Samples having thickness of about $0.1\,\mathrm{mm}$ could be treated as infinitely thick provided they contain significant amount of the heavy elements. Remaining dimensions of the sample are quite sufficient provided they are of the order of $3 \text{ x } 3\,\mathrm{mm}$.

3. DIFFUSION IN THE SIMPLE B2 STRUCTURE ALLOYS

B2 structure is basically a caesium chloride cubic structure with two vortices per chemical unit cell. A chemical unit cell can be considered as the BCC unit cell provided all atoms filling all vortices are of the same kind. Otherwise the structure has to be regarded as composed of two simple cubic Bravais sub-lattices interpenetrating each other and shifted one versus another by the half of the lattice constant a in each direction [37]. The vertex of the first sub-lattice has co-ordinates (000) in the main crystal frame, while the vertex of the second sub-lattice has co-ordinates $(\frac{1}{2}\frac{1}{2}\frac{1}{2})$ in the same reference frame. The B2 structure with the possible diffusion jumps is shown in the Fig. 4.

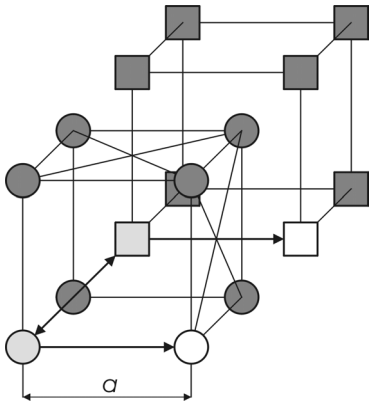

Fig. 4 B2 structure with the most probable routes of diffusion

A chemical formula of the binary alloy crystallising in the B2 structure can be expressed as A_xB_{1-x}. If one assumes that the symbol A denotes a minority component, while the symbol B denotes a majority component, one obtains the following constraint on the concentration $0 < x \leq \frac{1}{2}$ normalised to the unit cell. It is assumed here that no interstititials are present even at very high temperatures, and that the ground state is free of vacancies. Hence one of the sub-lattices is perfectly ordered in the ground state being filled completely by the majority component, while the other one is filled completely by the minority component and the remainder of the majority component, if present. The latter sub-lattice remains in the disordered state down to the atomic scale. Vacancies are created thermally and they occur as disordered mono-vacancies in both sub-lattices.

It is assumed that diffusion proceeds via uncorrelated mono-vacancy jumps. These jumps occur to the nearest neighbours either within the same sub-lattice or between sub-lattices. Hence the index $S = 2$ and the index $M = 3$ as there are three kind of "atoms", i.e., atoms of the component A, component B and thermally created mono-vacancies. In such a case a diffusion operator has dimensions $[6 \text{ x } 6]$ and it is composed of three $[2 \text{ x } 2]$ matrices in the form of a block matrix. Each of these matrices takes on the following form:

$$\mathbf{W}^{(m)} = \begin{bmatrix} -\omega_1^{(m)}[1-\alpha_1(\mathbf{q})] - \omega_{12}^{(m)} & \omega_{12}^{(m)}\alpha_{12}(\mathbf{q}) \\ \omega_{21}^{(m)}\alpha_{12}(\mathbf{q}) & -\omega_2^{(m)}[1-\alpha_1(\mathbf{q})] - \omega_{21}^{(m)} \end{bmatrix}. \tag{3.1}$$

The equilibrium condition leads to the relationship $\omega_{21}^{(m)} = \left(p_{m1}/p_{m2}\right)\omega_{12}^{(m)}$. On the other hand, geometrical factors can be expressed in the following way [38]:

$$\alpha_1(\mathbf{q}) = \tfrac{1}{3}[\cos(aq_1) + \cos(aq_2) + \cos(aq_3)] \text{ and } \alpha_{12}(\mathbf{q}) = \cos(\tfrac{1}{2}aq_1)\cos(\tfrac{1}{2}aq_2)\cos(\tfrac{1}{2}aq_3). \tag{3.2}$$

Here the symbols q_1, q_2 and q_3 denote projections of the wave-vector transfer on the main crystal axes $<100>, <010>$ and $<001>$, respectively. The index $m = 1$ denotes a minority component, $m = 2$ denotes the majority component and $m = 3$ denotes a vacancy. Each atomic jump generates a simultaneous vacancy jump in the opposite direction. Hence the vacancy jump frequencies have to satisfy the following relationships:

$$\omega_1^{(3)} = p_{11}\omega_1^{(1)} + p_{21}\omega_1^{(2)},\ \omega_2^{(3)} = p_{22}\omega_2^{(2)} + p_{12}\omega_2^{(1)} \text{ and } \omega_{12}^{(3)} = \left(p_{11}/p_{31}\right)\omega_{12}^{(1)} + \left(p_{21}/p_{31}\right)\omega_{12}^{(2)}. \tag{3.3}$$

Occupation probabilities are additionally constrained by the chemical composition in the following way $(p_{11} + p_{12})/(p_{21} + p_{22}) = x/(1-x)$.

If one assumes that the system remains in the equilibrium governed by the Boltzmann statistics occupation probabilities of the all six states involved can be calculated in terms of the activation energies. The following set of equations can be derived under this assumption and the additional assumption that in the infinite temperature limit half of the all states is vacant:

$$\begin{aligned} &p_{11} = C_1\, x[2 - \exp(-U_2/T)],\ p_{21} = C_1[1 - 2x + x\exp(-U_1/T)],\ p_{31} = C_1\exp(-V_1/T), \\ &p_{22} = C_2\, x[1 - \exp(-U_1/T)],\ p_{12} = C_2\, x\exp(-U_2/T),\ p_{32} = C_2\exp(-V_2/T), \\ &C_1 = \left(1 + x[\exp(-U_1/T) - \exp(-U_2/T)] + \exp(-V_1/T)\right)^{-1} \text{ and} \\ &C_2 = \left(1 - x[\exp(-U_1/T) - \exp(-U_2/T)] + \exp(-V_2/T)\right)^{-1}. \end{aligned} \tag{3.4}$$

Here the symbol T denotes ambient temperature, while the symbols V_1 and V_2 stand for the vacancy creation energy in the sub-lattice $s = 1$ and $s = 2$, respectively. The energy U_1 is non-negative energy required to transfer minority atom A from its own sub-lattice $s = 1$ to the anti-structure sub-lattice $s = 2$ of this atom. Finally the energy U_2 plays the same role for the majority atom B, while being transferred from the sub-lattice $s = 2$ to the sub-lattice $s = 1$. There are no vacancies in the ground state provided the following conditions are satisfied $V_1 > U_1$ and $V_2 > U_2$.

One has to note that the following two order parameters can be defined in each equilibrium state except the ground state free of vacancies $s_1 = p_{11} - p_{12}$ and $s_2 = p_{22} - p_{21}$. These parameters converge to unity while approaching the ground state for strictly stoichiometric samples only, i.e., for $x = \frac{1}{2}$. Such systems have the biggest coupling energy per mole. Otherwise some disorder remains even in the ground state.

Remaining jump frequencies can be calculated under the assumption that jumps occur as over the barrier jumps and that the classical principle of the energy equipartition applies. The last assumption is valid for heavy atoms. The following set of equations is obtained for the latter case:

$$\omega_1^{(1)} = w_1 \exp(-B_{11}/T),\ \omega_2^{(1)} = w_2 \exp(-B_{12}/T),$$
$$\omega_1^{(2)} = \sqrt{\frac{\mathrm{m}_1}{\mathrm{m}_2}}\, w_1 \exp(-B_{21}/T),\ \omega_2^{(2)} = \sqrt{\frac{\mathrm{m}_1}{\mathrm{m}_2}}\, w_2 \exp(-B_{22}/T),$$
$$\omega_{12}^{(1)} = w_3 \exp[-(U_2 + B_1)/T],\ \omega_{12}^{(2)} = \sqrt{\frac{\mathrm{m}_1}{\mathrm{m}_2}}\, w_3 \exp(-B_2/T),$$
$$w_1 = 6p_{31}\,\omega_0,\ w_2 = 6p_{32}\,\omega_0 \text{ and } w_3 = 8p_{32}\,\omega_0 . \tag{3.5}$$

Symbols m_1 and m_2 denote masses of the atoms A and B, respectively. The symbol ω_0 stands for the frequency of a jump originating in some vertex and ending in another vertex under the assumption that the infinite temperature limit applies. Barriers B_{11} and B_{12} describe jumps of the atom A within $s = 1$ and $s = 2$ sub-lattices, respectively. Such jumps originate in some vertex and end in any vertex of the nearest neighbour shell. Similar jumps of the atom B are described by the barriers B_{22} and B_{21}. The first barrier refers to the sub-lattice $s = 2$, while the second barrier refers to the sub-lattice $s = 1$. The barrier B_1 describes jumps of the atom A originating in the vertex of the sub-lattice $s = 2$ and ending in any vertex belonging to the nearest neighbour shell of the sub-lattice $s = 1$. Finally the barrier B_2 describes analogous jumps of the atom B originating in the sub-lattice $s = 1$ and ending in the sub-lattice $s = 2$. It can be assumed that all the parameters of the above outlined model depend weakly on a temperature except the vicinity of the melting point.

Diffusion coefficients of the respective components, i.e., atoms A, B and vacancies are scalars as the system has cubic symmetry. They obey the following relationship:

$$D_m = \frac{a^2\,(\frac{1}{2}\,p_{m1}\omega_1^{(m)} + \frac{3}{8}\,p_{m1}\omega_{12}^{(m)} + \frac{3}{8}\,p_{m2}\omega_{21}^{(m)} + \frac{1}{2}\,p_{m2}\omega_2^{(m)})}{2\,(p_{m1} + p_{m2})}. \tag{3.6}$$

One can expect some curvature of the Arrhenius plots as the system exhibits several activation energies.

The above model depends upon four energy levels U_1, U_2, V_1 and V_2; six energy barriers B_{11}, B_{12}, B_{21}, B_{22}, B_1 and B_2; limiting frequency ω_0; atomic mass ratio $\mathrm{m}_1/\mathrm{m}_2$; lattice constant a and the chemical composition x. It allows to calculate any of the properties concerned with the diffusion at any temperature significantly lesser than the melting point and for any wave-vector transfer. In order to simulate expected signals, one has to insert scattering amplitudes of the components A and B and one has to estimate recoilless fractions for the above components.

Generally estimation of the recoilless fraction is a quite involved task [39,40]. Here we are going to resort to a simple harmonic Debye approximation for a cubic symmetry. Anharmonic terms are essential to obtain fast diffusion, but generally they might remain small for the

heavy atoms even in the region of diffusion. One can further assume that a recoilless fraction of the particular atom is independent of the sub-lattice. In such a case one obtains the following relationship $f_{ms}(\mathbf{q}) = \exp(-q^2 < R^2 >_m)$, where $m = 1,2$. The mean squared displacement $< R^2 >_m$ can be expressed by the following relationship in the simple Debye model [36]:

$$< R^2 >_m = \left(\frac{3\hbar^2}{4\mathrm{m}_m k_B \theta_D^{(m)}} \right) \left\{ 1 + 4 \left(\frac{T}{\theta_D^{(m)}} \right)^2 \int_0^{\left(\frac{\theta_D^{(m)}}{T} \right)} dz \left(\frac{z}{\exp(z) - 1} \right) \right\}. \tag{3.7}$$

Here the symbols k_B and $\hbar$ denote the Boltzmann constant and the Planck constant divided by 2π, respectively. Usually one can assume that the Debye temperature $\theta_D^{(m)}$ is the same for both components, i.e., one can assume that the following relationship is satisfied $\theta_D^{(m)} = \theta_D$.

3.1. SCATTERING GEOMETRY FOR CUBIC SINGLE CRYSTALS

Wave-vector transfer components in the main crystal axes $< 100 >, < 010 >$ and $< 001 >$ can be expressed as $q_1 = q \sin\vartheta \cos\varphi$, $q_2 = q \sin\vartheta \sin\varphi$ and $q_3 = q \cos\vartheta$, where the angle ϑ stands for the polar angle, while the angle φ stands for the azimuthal angle. On the other hand, the main crystal co-ordinates making a right handed orthogonal system in the case of cubic crystals are oriented in some way in the device co-ordinates $\{xyz\}$ constituting another right handed orthogonal system having common origin with the crystal system. It is assumed that the incoming beam propagates along the axis z and the scattering occurs into the $[x,z]$ plane with the outgoing wave-vector $\mathbf{q}_1$ having positive projection on the axis x. One can assume that the condition $q_0 = q_1$ is satisfied, as the scattering is quasi-elastic. Here the symbol q_1 denotes wave number of the outgoing radiation. A common origin is chosen as the reciprocal lattice point responsible for the forward scattering. The situation is shown in the Fig. 5 together with several Breit-Wigner cells and the corresponding Ewald sphere.

In order to determine the wave-vector transfer one has to calculate the above polar and azimuthal angles in terms of the incoming wave-vector and scattering angle θ. Hence one has to apply a rotation transformation by the Eulerian angles $(\alpha\Omega\gamma)$ as shown in the inset of the Fig. 5. The meaning of the Eulerian angles is the following while transforming from the device to the crystal co-ordinates. One has to apply rotation by the right handed angle γ around the axis z, followed by another right handed rotation by the angle Ω around the new axis y, and concluded by the final right handed rotation by the angle α around the newest axis z. The basal vectors of the crystal co-ordinates can be expressed as follows:

$$| \mathbf{U}_1 > = \begin{bmatrix} 1 \\ 0 \\ 0 \end{bmatrix}, \; | \mathbf{U}_2 > = \begin{bmatrix} 0 \\ 1 \\ 0 \end{bmatrix} \text{ and } | \mathbf{U}_3 > = \begin{bmatrix} 0 \\ 0 \\ 1 \end{bmatrix}. \tag{3.8}$$

On the other hand, a unit vector along the scattering vector takes on the following form in the device co-ordinates $< \mathbf{Q} | = \left(\frac{1}{\sqrt{2\,(1-\cos\theta)}} \right) \left[-\sin\theta \quad 0 \quad 1-\cos\theta \right]$. Therefore the following scalar products can be defined $S_j = < \mathbf{Q} \,|\, \mathbf{R}(\alpha\Omega\gamma) \,|\, \mathbf{U}_j >$ with $j = 1,2,3$. Here the symbol $\mathbf{R}(\alpha\Omega\gamma)$ stands for the Eulerian rotation operator. The polar angle can be obtained as $\vartheta = a\cos(S_3)$. The azimuthal angle differs from zero provided the quantity $S_{12} = \sqrt{S_1^2 + S_2^2}$ satisfies the relationship $S_{12} > 0$. In such a case the azimuthal angle can be calculated as $\varphi = a\cos(S_1 / S_{12})$. One has to transform the last angle into the angle $\varphi \Rightarrow 2\pi - \varphi$ provided the following condition is satisfied $S_2 < 0$.

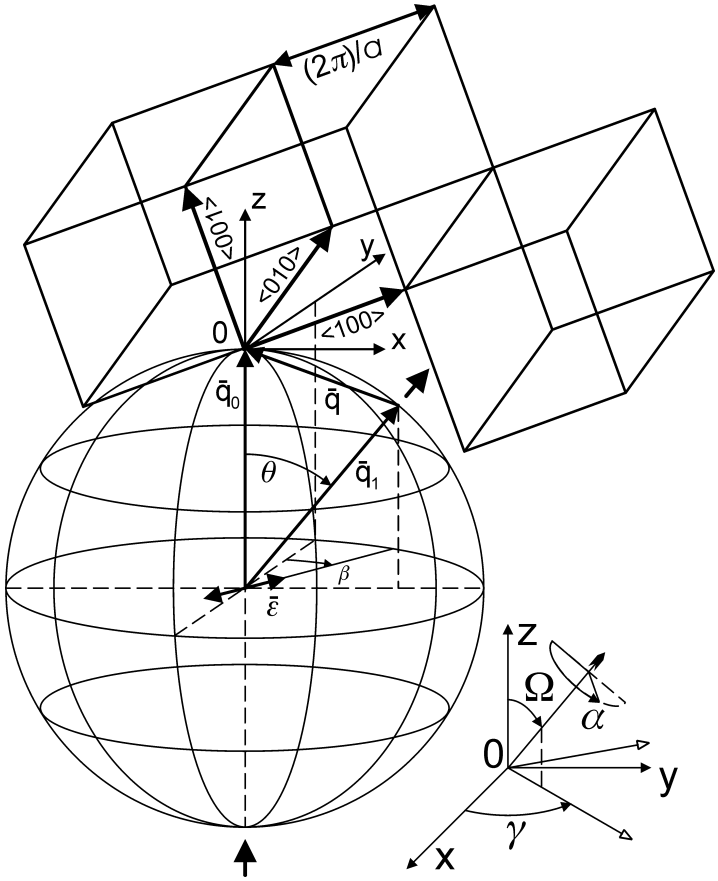

Fig. 5 Scattering geometry in the reciprocal space

The rotation operator takes on the following form:

$$\mathbf{R}(\alpha\Omega\gamma) = \begin{bmatrix} \cos\alpha\cos\Omega\cos\gamma - \sin\alpha\sin\gamma & -\cos\alpha\cos\Omega\sin\gamma - \sin\alpha\cos\gamma & \cos\alpha\sin\Omega \\ \sin\alpha\cos\Omega\cos\gamma + \cos\alpha\sin\gamma & -\sin\alpha\cos\Omega\sin\gamma + \cos\alpha\cos\gamma & \sin\alpha\sin\Omega \\ -\sin\Omega\cos\gamma & \sin\Omega\sin\gamma & \cos\Omega \end{bmatrix}. \tag{3.9}$$

Due to the fact that systems are disordered there are practically no forbidden Bragg reflections. In order to avoid Bragg reflections except forward scattering one can apply the following procedure. Namely the following vector can be defined:

$$|\mathbf{A}(hkl)>=\left(\frac{2\pi}{a}\right)\mathbf{R}(\alpha\Omega\gamma)[\,h\,|\mathbf{U}_1>+k\,|\mathbf{U}_2>+l\,|\mathbf{U}_3>]+q_0\,|\mathbf{U}_3>.$$

(3.10)

Here the indices (hkl) stand for the Miller indices. No Bragg condition is satisfied except the forward scattering condition provided the following inequality is satisfied for all possible sets of the Miller indices except $h=k=l=0$:

$$|\sqrt{<\mathbf{A}(hkl)\,|\,\mathbf{A}(hkl)>}-q_0\,|>\varepsilon_B q_0\,.$$

(3.11)

The parameter ε_B usually stays within the range $(10^{-3}-10^{-6})$ for reasonable single crystal including coherent inelastic scattering.

The experimental scattering arrangement is shown in the Fig. 6. It is assumed that one of the main crystal axes is perpendicular to the sample surface. A complete device beyond the movable resonant target can be rotated by some small angle around the axis y in order to set the angle χ between the incoming beam and the sample surface. Hence the angle γ satisfies the relationship $\gamma=0$, while the angle Ω can be calculated as $\Omega=\pi/2+\chi$. The third Eulerian angle α is the rotation angle around the main crystal axis perpendicular to the sample surface. This angle equals zero provided another main crystal axis is parallel to the axis y. The range of accessible scattering directions is shown in the Fig. 6 as well. A freedom to adjust the angle between the incoming beam and the sample surface is helpful in avoiding Bragg scattering.

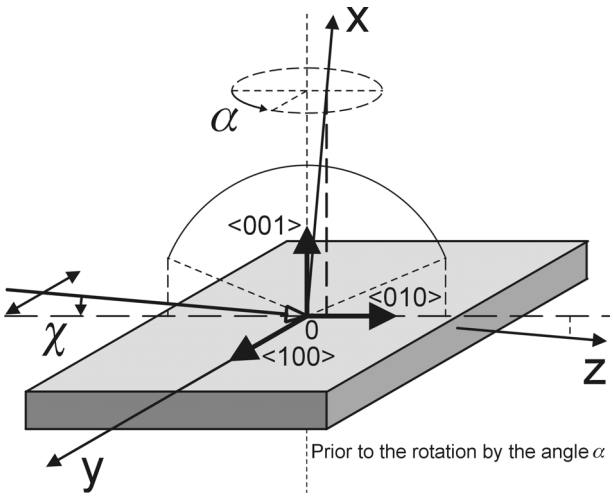

Fig. 6 The experimental scattering geometry

4. RESULTS OF SOME SIMULATIONS

Data patterns were simulated for the $Co_{0.627}Ga_{0.373}$ alloy single crystal [12]. Hence the component A denoted by $m=1$ is Ga, while the component B denoted by $m=2$ is Co. Essential parameters used to calculate data patterns are enclosed in Table 1 and 2. Scattering amplitudes were calculated by the relativistic Hartree-Fock method for metallic gallium and cobalt, respectively. Real parts of the scattering amplitudes $\eta_m(q_0\theta)$ are shown in the Fig. 7, while the imaginary parts $\chi_m(q_0)$ are enclosed in the Table 2. Energy levels and barriers of

the Table 2 are to be treated as the example as they do not necessarily correspond to the real quantities of the system considered. The same statement applies to the limiting jump frequency.

Table 1
Parameters of the X-ray interferometer

N_c	τ [ns]	ξ	q_0 [nm^{-1}]	v [mm/s]
1024	141	0	73	± 3
$\mu_1^{(R)} z_1$	$\mu_2^{(R)} z_2$	Δt [ps]	t_0 [ns]	T_R [ns]
12	12	200	4	700
θ [°]	α [°]	Ω [°]	γ [°]	β [°]
variable	variable	95	0	0

Table 2
Parameters of the sample

a [nm]	x	U_1 [K]	U_2 [K]	$V_1 = V_2$ [K]	B_{11} [K]
0.293	0.373	1600	1500	12000	9000
B_{12} [K]	B_{21} [K]	B_{22} [K]	B_1 [K]	B_2 [K]	ω_0 [s^{-1}]
8000	9500	10000	9300	7000	10^{13}
m_1 [AU]	m_2 [AU]	θ_D [K]	T [K]	$\chi_1(q_0)$	$\chi_2(q_0)$
69.7	58.9	430	variable	-0.0504	0.3212

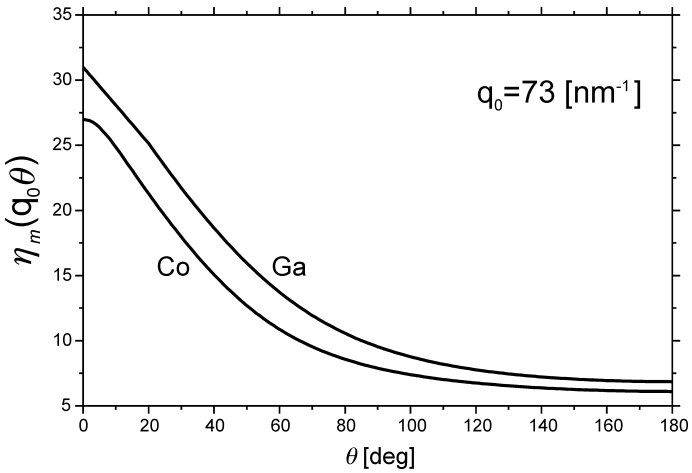

Fig. 7 Real parts of the scattering amplitudes plotted versus scattering angle

A correlation function $G(t)$ is plotted in the Fig. 8 for several temperatures. This function was calculated for the scattering angle $\theta = 40^o$ and for the angle $\alpha = 0$. Several intensities $I_M(t)$ calculated for the above set of angles are shown in the Fig. 9. These intensities were calculated varying temperature. On the other hand, intensities calculated for the temperature $T = 1300\,\mathrm{K}$ and various scattering angles are shown in the Fig. 10. These intensities were calculated for two distinctly different values of the angle α each. Prompt pulses are omitted for the above intensities.

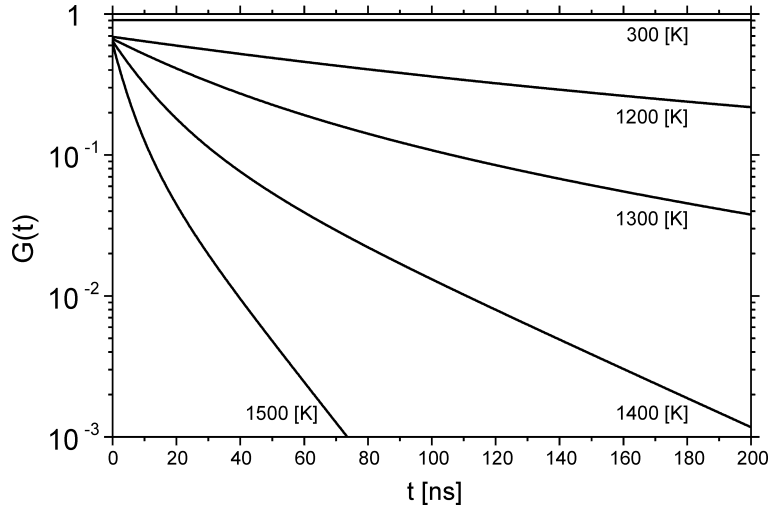

Fig. 8 Correlation function at various temperatures

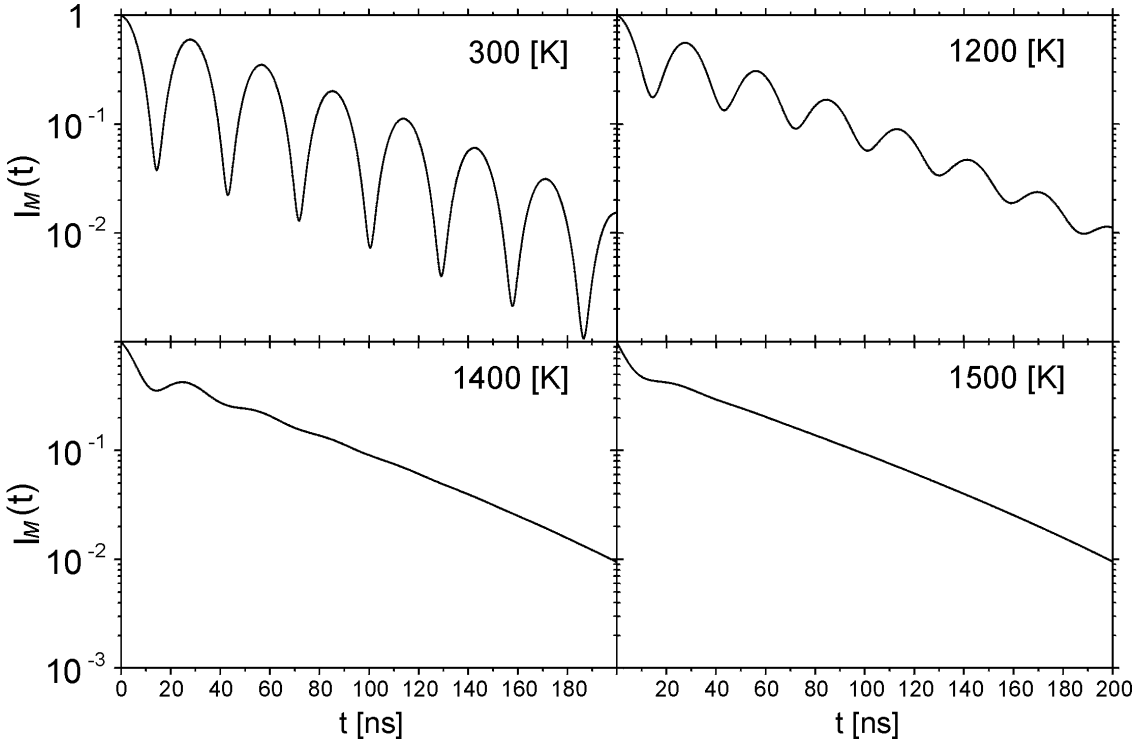

Fig. 9 Theoretical intensities at various temperatures

Finally Fig. 11 shows intensities $I_E(t)$ for the scattering angle $\theta = 20^o$ and two distinctly different values of the angle α calculated for the temperature $T = 1300\,\mathrm{K}$. These functions are obtained multiplying appropriate theoretical intensity by the scaling factor and applying statistical scatter of the same kind as produced by the photon counting device. Time scales of the photon counting device are applied too. A scaling factor was taken as $C_E = 10^4$.

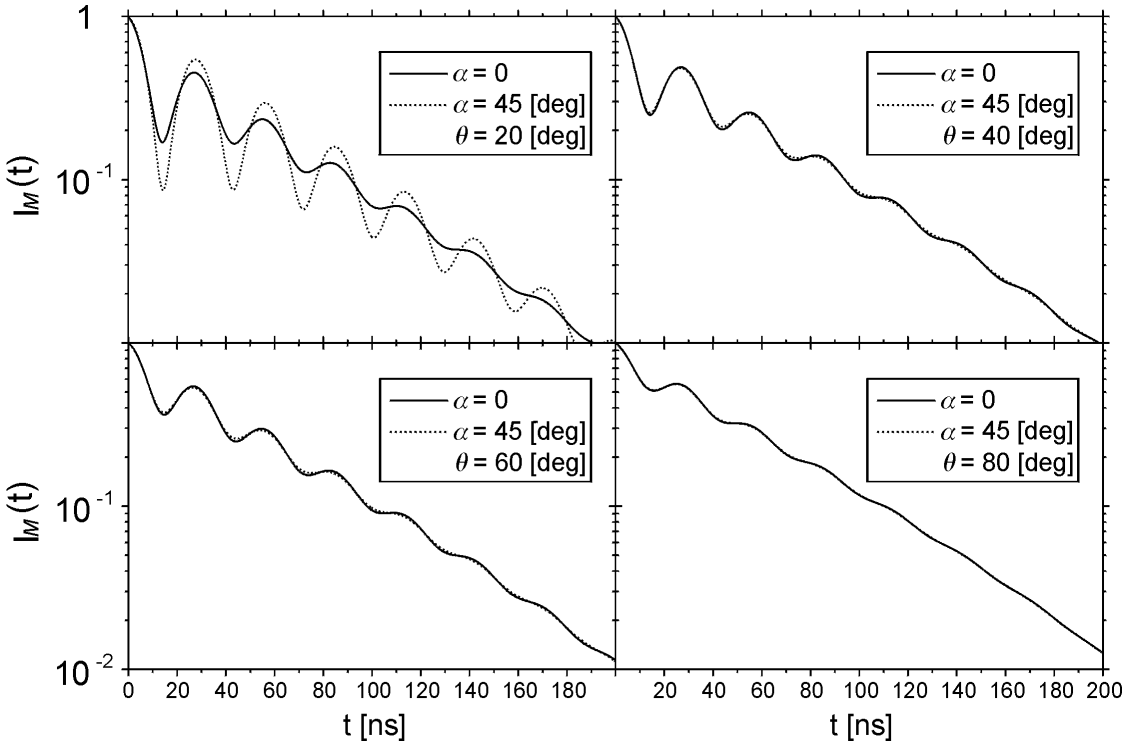

Fig. 10 Theoretical intensities for various scattering angles
Note that the direction having the following set of angles $\theta = 20^o$ and $\alpha = 45^o$ is a direction close to the Bragg reflection.

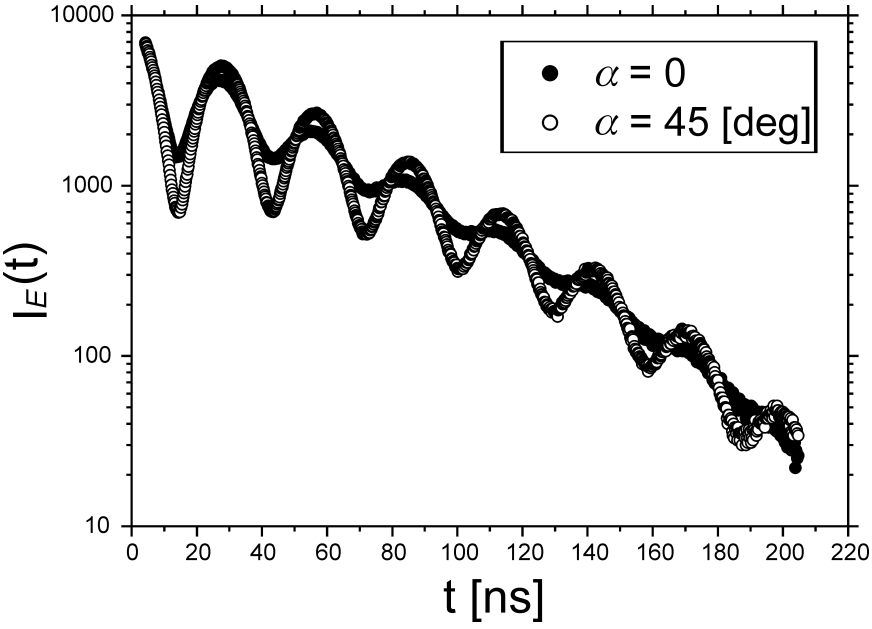

Fig. 11 Simulated intensities of the photon counting device

DISCUSSION AND CONCLUSIONS

It seems that the SGMR interferometry is going to be a powerful tool in investigation of the microscopic mechanisms of diffusion in partly disordered single crystals. It is essential to have significant disorder of atoms having vastly different atomic numbers between various

Bravais sub-lattices. A very good spatial resolution could be achieved at the energy resolution exceeding several orders of magnitude a resolution of the neutron scattering devices at the comparable spatial resolution. On the other hand, the energy resolution is much poorer than in the case of PCS. However PCS is unlikely to reach the spatial resolution of the SGMR interferometry and it is able to look at the very slow motions solely. Hence it is susceptible to the motion at the larger than atomic scale as well. SGMR interferometry is basically free of such artefacts. It looks at the atomic jumps in the very local scale. Hence even samples being far from the global equilibrium behave like samples being close to the equilibrium from the point of view of this method. Basically SGMR interferometry is similar to either emission or absorption quasi-elastic Mössbauer spectroscopy performed on the single crystalline samples [18,19]. Basic differences are due to the ability to change the wave number transfer in the case of the interferometry and to the ability to look upon non-resonant scattering centres. Actually resonant nuclei have to be absent in the sample investigated by the latter method. One has to note that all atoms in the sample contribute here to the correlation function albeit with various weights.

The biggest problem is to get sufficient count rate at the detector. The count rate is lowered due to the more or less isotropic character of the incoherent scattering by the sample and the necessity to use relatively small acceptance solid angle of the detector. The scattered intensity is further lowered by the high degree of the spatial order in the sample. These problems are likely to vanish by replacing undulators with the free electron lasers of the sufficient energy of the photon. The latter devices are going to concentrate the radiation intensity spread into the broad band in the case of undulators into a narrow band around the desired energy.

The application of the X-ray optics described above (or similar optics being equivalent) is essential to obtain reasonable data in the case of weakly scattering samples into the interesting channel. It is important to remove fluorescent and Compton scattered radiation from reaching the detector.

REFERENCES

1. Ruby, S.L. 1974 J. Phys. (Paris) Colloq., 35, C6-209.
2. Cohen, R.L., Miller, G.L., and West, K.W. 1978 Phys. Rev. Lett., 41, 381.
3. Gerdau, E., Rüffer, R., Winkler, H., Tolksdorff, W., Klages, C.P., and Hannon, J.P. 1985 Phys. Rev. Lett., 54, 835.
4. Hastings, J.B., Siddons, D.P., Faigel, G., Berman, L.E., Haustein, P.E., and Grover, J.R. 1989 Phys. Rev. Lett., 63, 2252.
5. Hastings, J.B., Siddons, D.P., van Bürck, U., Hollatz, R., and Bergmann, U., 1991 Phys. Rev. Lett., 66, 770.
6. Kikuta, S., Yoda, Y., Hasegawa, Y., Izumi, K., Ishikawa, T., Zhang, X.W., Kishimoto, S., Sugiyama, H., Matsushita, T., Ando, M., Suzuki, C.K., Seto, M., Ohno, H., and Takei, H. 1992 Hyperfine Interact., 71, 1992.
7. van Bürck, U., Siddons, D.P., Hastings, J.B., Bergmann, U., and Hollatz, R. 1992 Phys. Rev. B, 46, 6207.
8. Baron, A.Q.R., Franz, H., Meyer, A., Rüffer, R., Chumakov, A.I., Burkel, E., and Petry, W. 1997 Phys. Rev. Lett., 79, 2823.
9. Smirnov, G.V., Kohn, V.G, and Petry, W. 2001 Phys. Rev. B, 63, 144303.
10. Sepiol, B., Kaisermayr, M., Thiess, H., Vogl, G., Alp, E.E., and Sturhahn, W. 2000 Hyperfine Interact., 126, 329.

11. Kaisermayr, M., Sepiol, B., Thiess, H., Vogl, G., Alp, E.E., and Sturhahn, W. 2001 Eur. Phys. J., 20, 335.
12. Żmudzki, D. 2002 M. Sc. Thesis, Pedagogical University, Kraków.
13. Singwi, K.S., and Sjölander, A. 1960 Phys. Rev., 120, 1093.
14. Chudley, C.T., and Elliott, R.J. 1961 Proc. Phys. Soc. (London), 77, 353.
15. Rowe, J.W., Sköld, H.E., Flotow, H.E., and Rush, J.J. 1971 J. Phys. Chem. Solids, 32, 41.
16. Kutner, R., and Sosnowska I. 1977 J. Phys. Chem. Solids, 38, 741.
17. Kwater, M., Ruebenbauer, K., and Wdowik U.D. 1993 Physica B, 190, 199.
18. Petry, W., and Vogl, G. 1987 Mat. Sci. Forum, 15-18, 323.
19. Vogl, G. 1990 Hyperfine Interact., 53, 197.
20. Steinmetz, K.H., Vogl, G., Petry, W., and Schroeder, K. 1986 Phys. Rev. B, 34, 107.
21. Miczko, B., Ruebenbauer, K., and Sepiol, B. 1989 Hyperfine Interact., 52, 107.
22. Ruebenbauer, K., Sepiol, B., and Miczko, B. 1991 Physica B, 168, 80.
23. Ruebenbauer, K., Wdowik, U.D., and Kwater, M. 1996 Phys. Rev. B, 54, 4006.
24. Ruebenbauer, K., Wdowik, U.D., Kwater, M., and Kowalik, J.T. 1996 Phys. Rev. B, 54, 12880.
25. Ruebenbauer, K. 1998 Molecular Physics Reports, 22, 53.
26. Bée, M. 1988, Quasielastic Neutron Scattering, Adam Hilger, Bristol.
27. Mochrie, S.G.J., Mayes, A.M., Sandy, A.R., Sutton, M., Brauer, S., Stephenson, G.B., Abernathy, D.L., and Grübel, G. 1997 Phys. Rev. Lett., 78, 1275.
28. Pusey, P.N. 1991 Liquids, Freezing and Glass Transitions, J.P. Hansen, D. Levesque, and J. Zinn-Justin (Eds.), North Holland, Amsterdam.
29. Schupp, G., Hammouda, B., and Hsueh, C.M. 1990 Phys. Rev. A, 41, 5610.
30. Hammouda, B., and Schupp, G. 1990 J. Chem. Phys., 93, 5473.
31. Ruebenbauer, K., Mullen, J.G., Nienhaus, G.U., and Schupp, G. 1994 Phys. Rev. B, 49, 15607.
32. Baron, A.Q.R., and Ruby, S.L. 1994 Nucl. Instr. Meth., A343, 517.
33. Chumakov, A.I. 2001 private communication.
34. Schupp, G., Barnes, K., Yelon, W.B., and Mullen, J.G. 1991 private communication.
35. Górnicki, R., and Ruebenbauer, K. 2002 unpublished.
36. Greenwood, N.N., and Gibb, T.C. 1971 Mössbauer Spectroscopy, Chapman and Hall Ltd., London.
37. Stolwijk, N.A., van Gend, M., and Bakker, H. 1980 Philosophical Magazine, 42, 783.
38. Ruebenbauer, K., and Sepiol, B. 1986 Hyperfine Interact., 30, 121.
39. Ruebenbauer, K., and Wdowik, U.D. 2000 Phys. Rev. B, 61, 11416.
40. Wdowik, U.D., and Ruebenbauer, K. 2000 Molecular Physics Reports, 30, 137.